The Astrophysical Journal, 720:465–479, 2010 September 1 doi:10.1088/0004-637X/720/1/465
© 2010. The American Astronomical Society. All rights reserved. Printed in the U.S.A.

A SPECTROSCOPIC SEARCH FOR LEAKING LYMAN CONTINUUM AT $z \sim 0.7$*

Carrie R. Bridge[1], Harry I. Teplitz[2], Brian Siana[1], Claudia Scarlata[3], Christopher J. Conselice[4], Henry C. Ferguson[5], Thomas M. Brown[5], Mara Salvato[1,6], Gwen C. Rudie[1], Duilia F. de Mello[7,8], James Colbert[3], Jonathan P. Gardner[8], Mauro Giavalisco[5], and Lee Armus[3]
[1] California Institute of Technology, 220-6, Pasadena, CA 91125, USA; bridge@astro.caltech.edu
[2] Infrared Processing and Analysis Center, MS 100-22, Caltech, Pasadena, CA 91125, USA
[3] Science Center, California Institute of Technology, 220-6, Pasadena, CA 91125, USA
[4] University of Nottingham, Nottingham, NG7 2RD, UK
[5] Space Telescope Science Institute, 3700 San Martin Drive, Baltimore, MD 21218, USA
[6] Max-Planck institute for Plasma Physics & Excellence Cluster Boltzmans strasse 2, Garching 86748, Germany
[7] Department of Physics, Catholic University of America, 620 Michigan Avenue, Washington, DC 20064, USA
[8] Astrophysics Science Division, Observational Cosmology Laboratory, Code 665, Goddard Space Flight Center, Greenbelt, MD 20771, USA
Received 2010 March 17; accepted 2010 July 7; published 2010 August 11

ABSTRACT

We present the results of rest-frame, UV slitless spectroscopic observations of a sample of 32 $z \sim 0.7$ Lyman break galaxy (LBG) analogs in the COSMOS field. The spectroscopic search was performed with the Solar Blind Channel on the *Hubble Space Telescope*. We report the detection of leaking Lyman continuum (LyC) radiation from an active galactic nucleus–starburst composite. While we find no direct detections of LyC emission in the remainder of our sample, we achieve individual lower limits (3σ) of the observed non-ionizing UV-to-LyC flux density ratios, f_ν (1500 Å)/ f_ν(830 Å) of 20 to 204 (median of 73.5) and 378.7 for the stack. Assuming an intrinsic Lyman break of 3.4 and an intergalactic medium transmission of LyC photons along the line of sight to the galaxy of 85%, we report an upper limit for the *relative* escape fraction in individual galaxies of 0.02–0.19 and a stacked 3σ upper limit of 0.01. We find no indication of a relative escape fraction near unity as seen in some LBGs at $z \sim 3$. Our UV spectra achieve the deepest limits to date at any redshift for the escape fraction in individual sources. The contrast between these $z \sim 0.7$ low escape fraction LBG analogs with $z \sim 3$ LBGs suggests that either the processes conducive to high $f_{\rm esc}$ are not being selected for in the $z \lesssim 1$ samples or the average escape fraction is decreasing from $z \sim 3$ to $z \sim 1$. We discuss possible mechanisms that could affect the escape of LyC photons.

Key words: cosmology: observations – galaxies: evolution – ultraviolet: galaxies

Online-only material: color figures

1. INTRODUCTION

Reionization brought an end to the cosmic "dark ages," during which the universe contained a mostly neutral intergalactic medium (IGM). This transition is thought to be triggered by either the radiation from QSOs or from galaxies containing large populations of massive stars. Recent determinations of the high-redshift QSO luminosity function suggest that QSO space densities are too low to reionize the universe at $z > 6$ (Willott et al. 2010; Brusa et al. 2009; Siana et al. 2008; Jiang et al. 2008), with the exception of Glikman et al. (2010). The contribution of galaxies to the ionizing UV background (Madau et al. 1999) depends upon how many of the Lyman continuum (LyC) photons produced by massive young stars escape a galaxy, evading absorption by neutral hydrogen atoms or dust grains. Direct measurement of the escape fraction, $f_{\rm esc}$, is impossible at the epoch of reionization, because intervening absorbers make the IGM opaque to LyC photons. Instead, $f_{\rm esc}$ must be measured at lower redshifts ($z \lesssim 3.5$) in objects that are analogous to the galaxies responsible for reionization.

Detection of escaping LyC photons has eluded most surveys. Observations of Lyman break galaxies (LBGs) at $z \sim 3$ (Steidel et al. 2001; Shapley et al. 2006; Iwata et al. 2009) suggest that in ∼10% of starbursts the escape fraction is quite large, nearing unity. In contrast, there are currently no LyC detections locally ($z \lesssim 1$), despite tremendous effort (Leitherer et al. 1995; Giallongo et al. 1997; Deharveng et al. 2001; Malkan et al. 2003; Siana et al. 2007; Cowie et al. 2009, see Siana et al. 2010 for a review). One explanation suggested by several authors is that the cosmic average escape fraction evolves with redshift (Inoue et al. 2006; Siana et al. 2007, 2010). One notable difference between high- and low-redshift studies of the escape fraction is the wavelength range used to measure the LyC flux. All previous surveys searching for intermediate redshift LyC leaking galaxies have utilized broadband photometry which probe ∼700 Å while $z \sim 3$ studies measure the LyC just below the Lyman limit. Probing these shorter wavelengths increases the sensitivity to the star formation history, dust extinction, and IGM absorption. This means a decrease in star formation within the last 10 Myr would significantly lower the flux at 700 Å compared to 900 Å, weakening the LyC limits measured from broadband photometry. It is with this difference in mind that we have undertaken a large spectroscopic program with the *Hubble Space Telescope* (*HST*) to study the escape fraction in luminous starbursts at $z \sim 0.7$ (GO 11236; PI: Teplitz).

Using the Solar Blind Channel (SBC) of the Advanced Camera for Surveys (ACS), we have obtained far-ultraviolet (FUV) spectra of 32 starbursts chosen to be good analogs of LBGs. The observations presented in this paper cover rest frame ∼750–1100 Å, and provide the first spectroscopic search for LyC photons from galaxies at $0 < z < 3$, as well as the deepest limits on the escape fraction for individual galaxies at

* Based on observations made with the NASA/ESA *Hubble Space Telescope*, obtained at the Space Telescope Science Institute, which is operated by the Association of Universities for Research in Astronomy, Inc., under NASA contract NAS 5-26555. These observations are associated with program 11236.

any redshift. Spectroscopy has an advantage over broadband imaging by being able to probe closer to the Lyman limit (up to 880 Å versus 700 Å), while being on board *HST* provides high spatial resolution making it possible to study any offset of LyC radiation compared to UV emission. The large sample size provides enough number statistics to make a meaningful comparison with the rare, high-z, LBG detections.

While no LyC flux is conclusively detected (excluding the detection in an active galactic nucleus–starburst galaxy), we use these spectra to place strict limits on the UV (∼1025 Å) to LyC (780–860 Å) ratio and infer the limit on the escape fraction of ionizing photons. In Section 2, we describe the selection of LBG-analog targets; in Section 3, we present the observations and data reduction. The method of measuring limits on the escape fraction is presented in Section 4. In Sections 5 and 6, we give the results and discuss their implications. A cosmology of $\Omega_M = 0.3, \Omega_\Lambda = 0.70$, and $H_0 = 70$ km s^{-1} Mpc^{-1} is assumed throughout.

2. SAMPLE SELECTION

Our aim was to choose galaxies at moderate redshift that are analogs to the $z \sim 3$ LBG population, which is conventionally taken as accessible analogs to $z > 6$ galaxies. Probing $z \sim 1$ analogs provides the opportunity for a wide range of observations, together with the opportunity to study the possible evolution of the escape fraction with redshift. Hoopes et al. (2007) demonstrated the similarity between LBGs and the compact subset of local UV luminous galaxies (UVLG; Heckman et al. 2005). These sources share many properties with LBGs including luminosity, size, specific star formation rate (SFR), mass, and metallicity (Heckman et al. 2005). The compact UVLG population is quite rare locally (about 1 per square degree at $z < 0.3$), but its numbers increase with redshift. They are identified by their UV luminosity ($L > 2 \times 10^{10}\ L_\odot$) and surface brightness ($I_{FUV} > 10^8\ L_\odot$ kpc^{-2}; Hoopes et al. 2007).

The wavelength range of the SBC/PR130L configuration limits the redshift range in which we can measure the LyC to $0.6 < z < 0.85$. Furthermore, SBC prism spectra are slitless, introducing a smearing effect, whereby the spectral resolution is degraded proportionally to the spatial extent of the target. Thus, we further restricted our selection to compact galaxies, which is in line with the LBG-analog selection.

To choose appropriate targets, we needed access to deep UV photometry, good redshift estimates, and a measure of compactness and surface brightness. These three data sets are available in the COSMOS field (Scoville et al. 2007). We derived the UV luminosity from *Galaxy Evolution Explorer* (*GALEX*) photometry (Zamojski et al. 2007), the size from *HST* (F814W) imaging (Koekemoer et al. 2007), and an accurate photometric redshift with the COSMOS 30+ band photometry (Mobasher et al. 2007).

We selected non-point sources with large L_{FUV} and I_{FUV} analogous to LBGs (Figure 1). After visual inspection, we discarded 15 sources for technical reasons not obvious in the catalog, such as a close proximity to the edge of the *GALEX* field of view which suffers from artifacts. There are 32 sources remaining that meet our criteria. These sources are the brightest UV galaxies at $z \sim 0.7$, but their luminosity ($\log L_{UV} \gtrsim 10.4\ L_\odot$) is similar to that of typical LBGs at $z \sim 3$. An $\sim L*$ galaxy at $z > 6$ would fall at the faint end of the same range. The UV luminosity of the targets corresponds to an SFR of 8–45 $M_\odot$ yr^{-1}, without correcting for dust extinction.

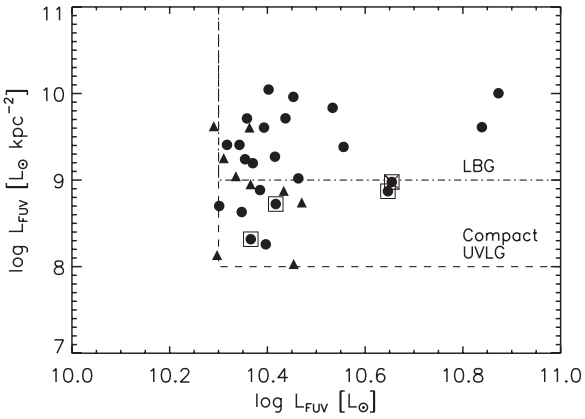

Figure 1. FUV luminosity vs. FUV surface brightness for our sample of 32 galaxies (circles and triangles) with $0.65 < z < 0.85$ in COSMOS. The dash-dotted line indicates the region occupied by $z \sim 3$ LBGs (Hoopes et al. 2007; Giavalisco 2002), while the dashed line marks the region occupied by local compact UV luminous galaxies, thought to be analogs for $z \sim 3$ LBGs (Hoopes et al. 2007). The triangles highlight the galaxies that were not detected in the SBC prism observations. The open squares indicate galaxies with no ACS imaging, and the "×" (within a square) notes the target found to be an AGN–starburst composite (C-UVLG-17). Note that the angular sizes of our galaxies are derived using rest-frame optical ACS images, which are typically larger than the sizes measured by rest-frame UV images as in the case of Hoopes et al. (2007).

The 32 selected galaxies (Figure 2) share many observable properties with LBGs. By inference, they are the rare, young, strongly star-forming objects at moderate redshift that have just reached an evolutionary stage that was common at $z \sim 3$.

3. OBSERVATIONS AND REDUCTIONS

3.1. Slitless UV Spectroscopy

The SBC uses a Multi-Anode Microchannel Array (MAMA) that has no read noise and is not sensitive to cosmic rays. Targets were positioned to land on the lower right quadrant of the detector to minimize the dark current "glow," which was noted by Teplitz et al. (2006) to increase with exposure time.

The SBC field of view is $31'' \times 35''$, with a plate scale of $0\farcs032$ pixel^{-1}. The SBC PR130L, which covers 1250–2000 Å with a variable dispersion from 1.65 Å pixel^{-1} at 1250 Å to 20.2 Å pixel^{-1} at 1800 Å, is used because it is not sensitive to the Lyα airglow which dominates the background in the PR110L prism. The PR130L prism is still sensitive to other airglow lines so the observations were taken with the SHADOW constraint reducing the airglow by a factor of 10.

The sources have a median *GALEX* near-UV magnitude of 22.5 (AB), and required 1–4 *HST* orbits in the shadow position (1500 s/orbit; see Table 1 for details). Direct imaging (two 480 s exposures/orbit) of our targets at 1600 Å was also acquired in the same visit with the F150LP filter to establish a zero point of the wavelength scale. These data were taken over 2007 December–2009 January in Cycle 16. An example of the direct SBC image and corresponding two-dimensional spectra is shown in Figure 3 for a typical starburst galaxy in our sample and the target which is an AGN–starburst composite (also see Figure 4 and Section 5.1 for a discussion).

The flat-fielding and dark subtraction of the SBC data were performed by the *HST* pipeline. Since this work relies on the measurement of flux below the Lyman limit, and our observations are background limited, sky subtraction must be done with care. The mean value for a region of sky, typically 300 pixels × 150 pixels above and below the target, is measured

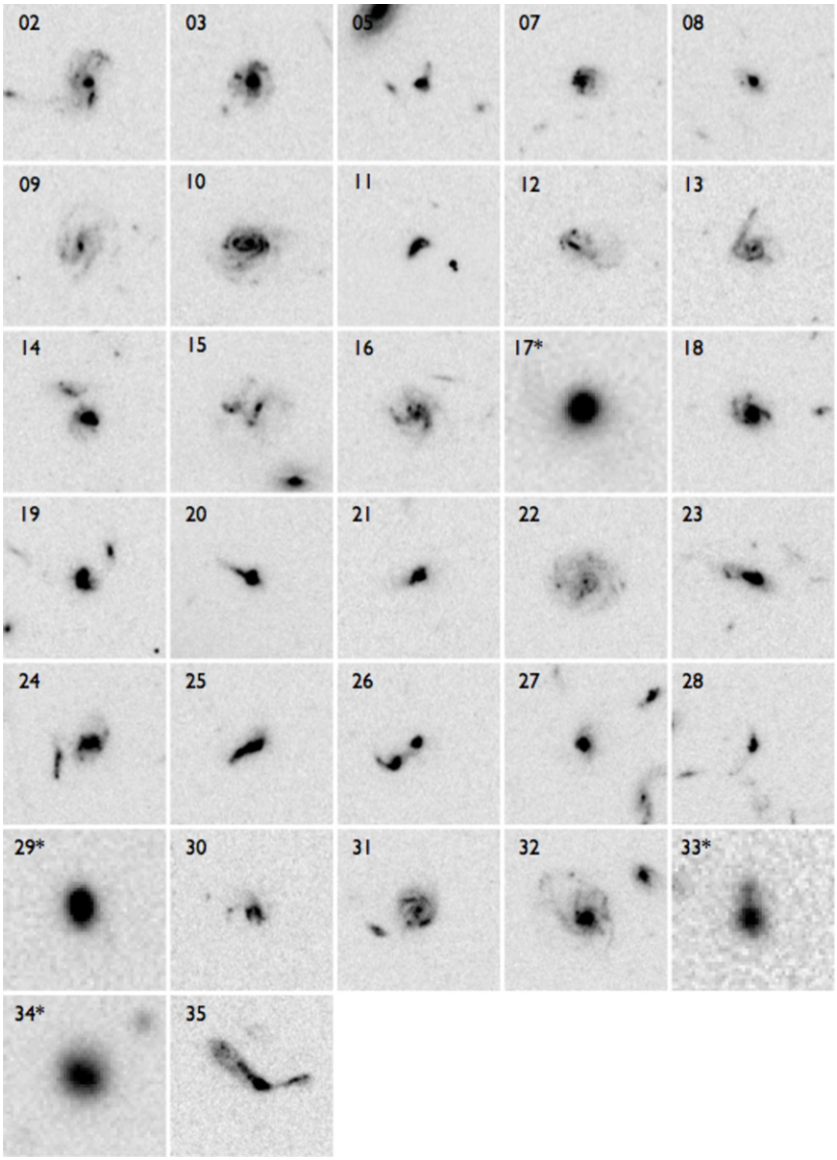

Figure 2. Optical images of the 32 $z \sim 0.7$ LBG analogs. Thumbnails are F814W *HST* images except those marked with an asterisk (Nos. 17, 29, 33, 34), which are CFHT ground-based i'. The images are 7″ on a side, with the object ID noted in the left corner.

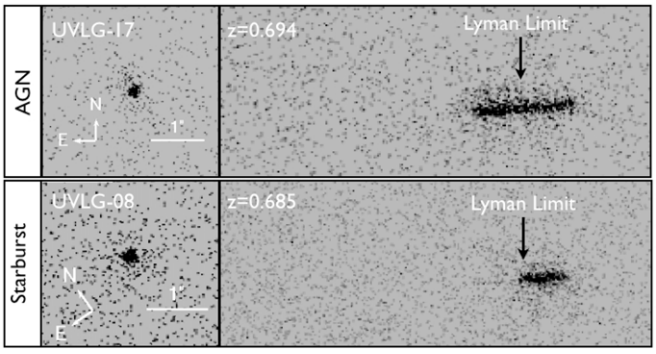

Figure 3. Example of the SBC F150LP direct UV image (left) and two-dimensional spectra (right) of an AGN (UVLG-17) and a starburst galaxy (UVLG-08) in our sample. The Lyman limit is noted in each spectra. Flux below 912 Å is clearly detected in the AGN, while no LyC detection is found in the starburst galaxy. Wavelength increases from the left to right covering ∼1220–2000 Å observed.

for each prism exposure. The average sky background in each individual exposure is subtracted from each flat-fielded prism image. The spectra were extracted in PyRAF using the *aXe* slitless spectroscopy reduction package (ver. 1.6; Walsh et al. 2006; Kümmel et al. 2006), specifically designed for *HST* grism and prism data.

In the extraction, the position of the galaxy on the direct image is used in combination with the header dither parameters to locate the spectrum on the dispersed image and assign a wavelength to each pixel in the spectrum. The spectral trace and wavelength solutions are defined with respect to a reference position, which is measured by running SExtractor (Bertin & Arnouts 1996) on a direct image for each orbit. A master catalog was generated for each set of prism images taken in a single orbit. Using the master catalogs, the *aXe* software generates pixel extraction tables (PETs), which contain a spectral mapping for each pixel in the spectrum. Various sizes for the extraction window were explored, with an extraction width approximately the size of the object maximizing the

Table 1
SBC Observations of LBG Analogs in the COSMOS Field

Object ID	R.A.	Decl.	Exp. Time	z_{spec}	NUV[a]	$f_\nu 830$[b]	$(f_\nu 1500/f_\nu 830)_{obs}$[c]	$f_{esc,rel}$[d]	$f_{esc,rel}$[e]
C-UVLG-02	149.94569	2.50422	108	0.667	22.40	2.880e-19	36.90	<0.108	<0.223
C-UVLG-05	150.08705	2.30905	108	0.688	22.60	1.708e-17	118.94	<0.034	<0.069
C-UVLG-07	150.21405	2.36754	108	0.669	22.69	9.144e-16	73.45	<0.054	<0.112
C-UVLG-08	150.42432	2.03343	81	0.685	22.35	7.305e-20	144.16	<0.028	<0.057
C-UVLG-11	150.15372	1.84970	108	0.670	22.39	6.471e-17	112.37	<0.036	<0.073
C-UVLG-12	149.85553	2.55685	108	0.665	22.50	1.054e-16	20.69	<0.193	<0.397
C-UVLG-15	150.27368	2.55358	108	0.715[e]	22.60	3.243e-21	40.49	<0.099	<0.203
C-UVLG-18	150.60126	2.71238	108	0.676	22.53	1.671e-16	34.02	<0.118	<0.242
C-UVLG-19	150.48743	2.15107	108	0.684	22.41	4.484e-20	34.73	<0.115	<0.237
C-UVLG-20	150.51077	2.75674	81	0.675	22.09	5.094e-19	9312	<0.043	<0.088
C-UVLG-21	149.62891	2.19084	108	0.701	22.46	2.034e-16	161.10	<0.025	<0.051
C-UVLG-23	149.88934	2.73473	27	0.709	21.41	8.128e-19	203.56	<0.019	<0.040
C-UVLG-24	150.17247	2.63495	108	0.752	22.43	1.660e-16	36.05	<0.111	<0.228
C-UVLG-25	149.62904	1.66577	81	0.671	22.02	1.182e-20	74.98	<0.053	<0.109
C-UVLG-26	149.60760	2.16737	108	0.676	22.28	6.302e-19	121.33	<0.033	<0.068
C-UVLG-27	149.69514	2.74294	108	0.652	22.52	1.015e-19	82.99	<0.048	<0.099
C-UVLG-28	150.45580	1.65284	81	0.657	22.66	4.344e-19	33.84	<0.118	<0.243
C-UVLG-29	149.46870	2.58616	81	0.704	21.94	1.005e-18	66.43	<0.060	<0.124
C-UVLG-30	149.51488	1.89228	108	0.694	22.56	8.146e-17	50.50	<0.079	<0.163
C-UVLG-33	150.76311	2.80412	108	0.693	22.37	3.299e-19	124.97	<0.032	<0.065
C-UVLG-34	150.69376	2.84451	108	0.738	22.68	8.607e-17	62.97	<0.063	<0.130
C-UVLG-35	149.69348	2.59921	27	0.678	21.35	1.490e-18	72.07	<0.055	<0.114
Stack	(18 galaxies)[f]			0.685	22.14	6.379e-19	378.7	<0.011	<0.022
Stack	(8 mergers)[g]			0.678	22.50	1.249e-18	223.2	<0.018	<0.037

Notes. The values presents are 3σ limits. Objects 3, 9, 10, 13, 14, 16, 22, 31, and 32 were not detected in the FUV direct image, target 17 was an AGN.

[a] NUV magnitude from *GALEX* public release version 3.

[b] 3σ upper limits in units of erg s^{-1} cm^{-2} $Å^{-1}$.

[c] 3σ lower limits.

[d] Assumes an intrinsic flux ratio of $(f_{1500}/f_{830})_{int} = 3.4$ based in part from Steidel et al. 2001.

[e] Assumes $(f_{1500}/f_{830})_{int} = 7$ (Siana et al. 2007).

[f] Photometric redshift.

[g] All objects except 2, 7, 15, and 18 are included in the stack due to their extended sizes.

[h] Mergers that were compact with optimal dispersion directions: objects 5, 12, 19, 25, 26, 28, 30, and 35.

signal to noise of the spectra. The signal to noise was further increased (a factor of ∼1.4) by using *aXe's* optimal weighting extraction, which weights the pixels as a function of distance from the spectral trace rather than giving each pixel the same weight when generating the one dimensional spectra. The wavelength solution over 1300–1700 Å is accurate to within a few angstroms. The spectra were flux calibrated using the standard sensitivity curve for the PR130L prism (Larsen et al. 2006).

The flux- and wavelength-calibrated spectra for each prism image were co-added weighting each exposure by the rms of the background in each individual exposure. This was done to account for increasing dark current with subsequent exposures. For an individual target the dark current was a factor of 4 higher in the fourth orbit compared to the first. The uncertainty in the spectral flux was estimated differently for the wavelength regions redward and blueward of the Lyman limit. Blueward of 912 Å, where we typically measured no signal (i.e., no detection of LyC) we are essentially probing the background. We extracted regions of blank sky and found that the standard deviation of the sky flux between the observed wavelengths typically used to measure the LyC in our $z \sim 0.7$ sample was comparable to the standard deviation of the flux in our galaxies. We therefore use the standard deviation of the flux between the 780 and 860 Å rest frame (the region used to measure LyC flux limits) as a conservative estimate of the uncertainty. However, redward of the Lyman break, where flux is detected, the errors at each wavelength bin in the final one-dimensional co-added spectra are the 1σ *weighted* standard deviation since there were larger. The final one-dimensional spectra are presented in Figure 5.

3.2. Optical Spectroscopy

Accurate spectroscopic redshifts are required to identify the observed wavelengths corresponding to the rest-frame Lyman limit and LyC. Redshifts cannot be measured from the FUV spectra themselves since the prism probes blueward of Lyα in the rest frame and the resolution is too poor for the identification of absorption lines. The photometric redshifts, although sufficient for selection purposes, have an uncertainty corresponding to ∼200 Å at $z \sim 0.7$. Optical spectroscopy for six of our targets were taken from the public zCOSMOS program[9] (Lilly et al. 2009). An additional 23 spectra were obtained at the Palomar Hale 5 m Telescope using the Double Spectrograph (hereafter Double Spec; Oke & Gunn 1982) in 2008 and 2009 February with seeing conditions ranging from 1″ to 2.″5 for the majority of the observations and light cirrus. This instrument uses a pair of CCD cameras that simultaneously obtain long-slit spectra over a "blue" range of 3500–5600 Å and a "red" range of 6000–8500 Å. The observing strategy consisted of acquiring

[9] Based on zCOSMOS observations carried out using the Very Large Telescope at the ESO Paranal Observatory under program ID: LP175.A-0839.

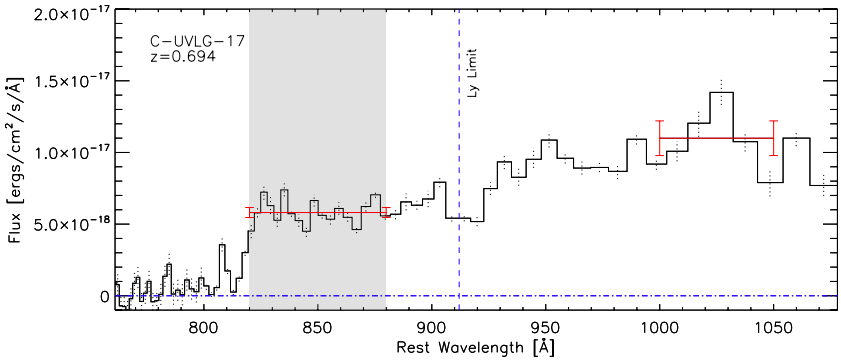

Figure 4. Individual spectrum of galaxy C-UVLG-17. Below the Lyman limit UV flux is clearly detected, showing that if LyC photons were escaping at the ∼15% level it would be detected by our observations. The source of these photons is likely the Type 2 AGN.

(A color version of this figure is available in the online journal.)

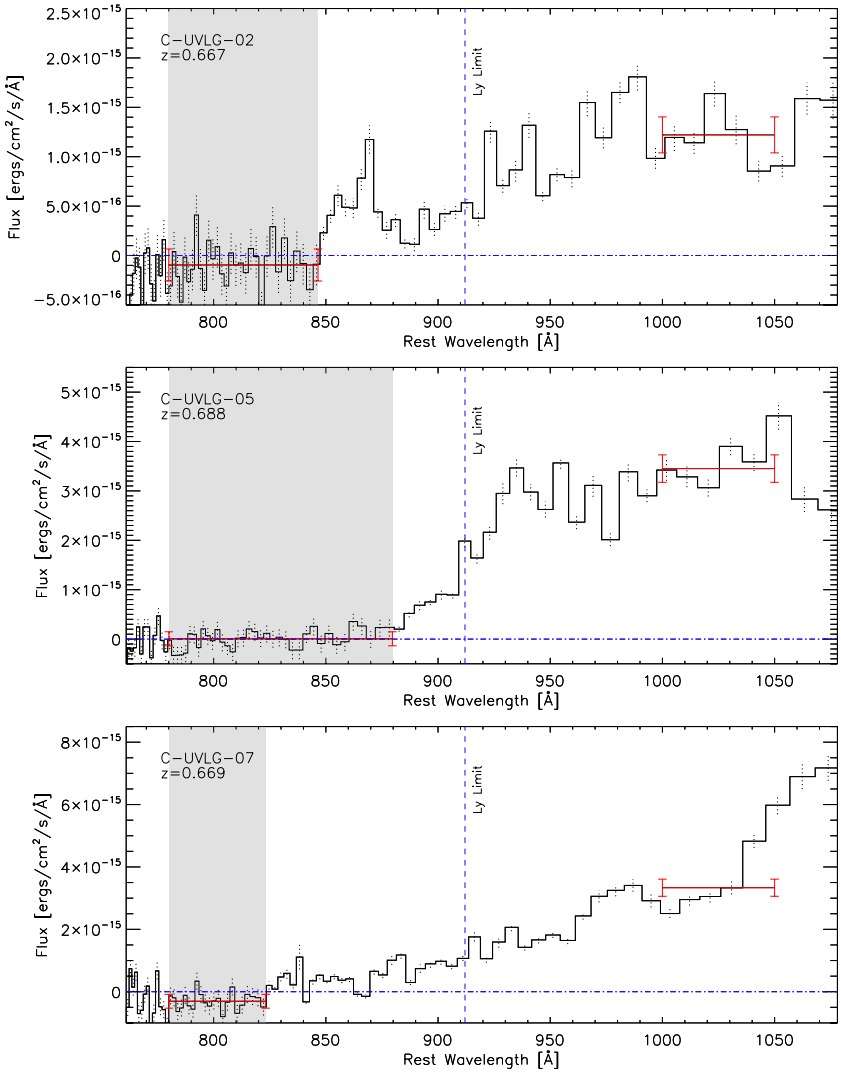

Figure 5. Deep UV slitless spectra of $z \sim 0.7$ LBG analogs in the COSMOS field. The spectra have been shifted into the rest frame and fluxes are in erg cm^{-2} s^{-1} Å^{-1}. The horizontal lines (red) represent the average flux over two wavelength ranges, ∼780–880 Å and 1000–1050 Å with 3σ error bars.

(A color version of this figure is available in the online journal.)

a series of 600–900 s exposures with a slit width of 1.″5. We obtained a total integration time of 40–90 minutes for each of the 23 galaxies.

The data were reduced using standard IRAF tasks and wavelength calibrated with He, Ne, and Ar reference lamps. The spectral features used for the redshift determination were typically a combination of O[II] at 3727 Å, O[III] at 5007 Å and in some cases Hβ at 4861 Å. The spectroscopic redshifts confirmed that all the observed galaxies were within the $0.6 < z < 0.85$ range needed to measure the escape fraction with the

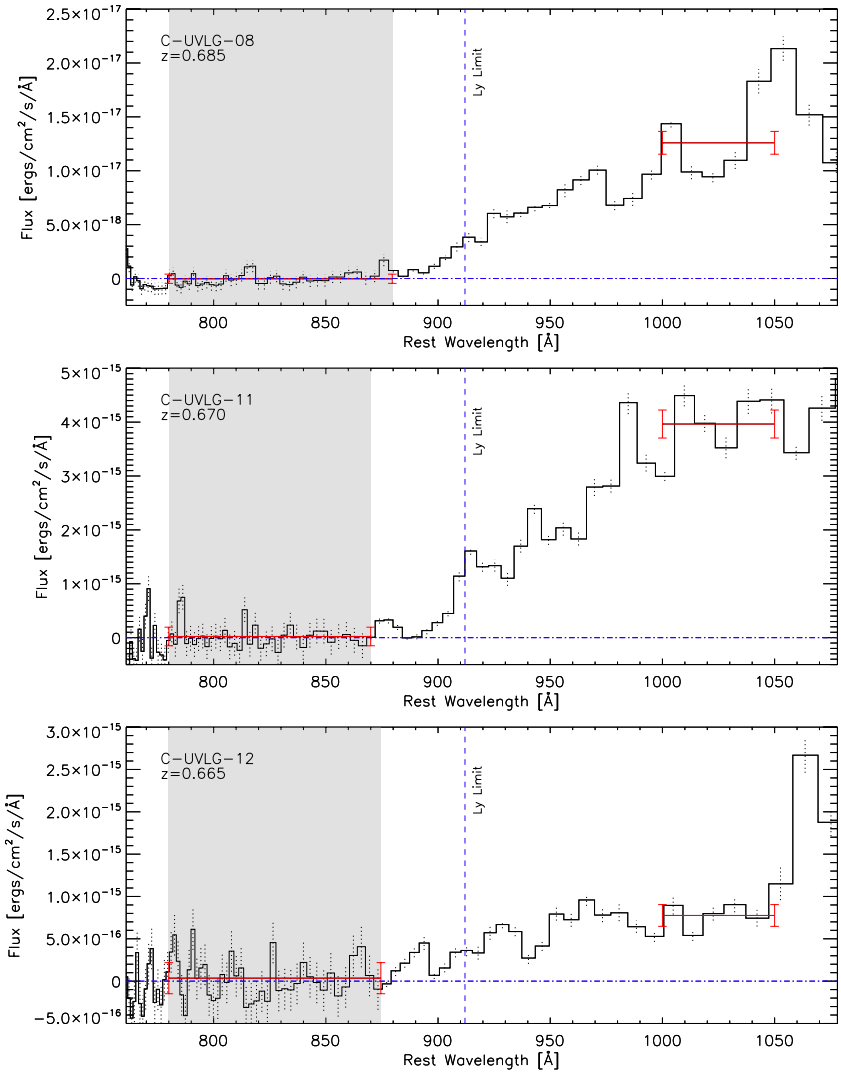

Figure 5. (Continued)

UV observations. The mean spectroscopic redshift of the sample is $z = 0.679$. Due to poor observing conditions, three targets remain with no spectroscopic redshift confirmation. Since only one of these (C-UVLG-15) had a detectable UV spectrum and the rest of the sample had photometric redshifts within a few percent of the spectroscopic redshift we assumed the photometric redshift for this galaxy.

4. DERIVING THE ESCAPE FRACTION

Typically, the escape fraction of LyC photons is measured relative to the number of photons escaping at $\lambda_{\rm rest} = 1500$ Å (Steidel et al. 2001). This allows a straightforward calculation of the escape fraction with only two flux measurements (at 1500 Å and in the LyC) using the following equation:

$$f_{\rm esc,rel} = \frac{(f_{1500}/f_{\rm LyC})_{\rm int}}{(f_{1025}/f_{\rm LyC})_{\rm obs} \times (S)} \times \exp(\tau_{\rm IGM,LyC}), \qquad (1)$$

where $(f_{1500}/f_{\rm LyC})_{\rm int}$ and $(f_{1025}/f_{\rm LyC})_{\rm obs}$ are the intrinsic and observed LyC flux density ratios. The "LyC" refers to the wavelength at which LyC is measured (780–860 Å for this study), S is the scaling factor discussed below, and $\tau_{\rm IGM,LyC}$ is the IGM optical depth for LyC photons along the line of sight to the galaxy. The intrinsic drop between the rest-frame FUV (1500 Å) and the LyC (700–900 Å) is highly uncertain and cannot be observed. The assumed value of $f_\nu(1500\ {\rm Å})/f_\nu({\rm LyC})$ has varied by study from 3 (Steidel et al. 2001; Shapley et al. 2006) to 6 or 8 (Siana et al. 2007).

Since we probe LyC radiation at slightly bluer wavelengths, at 830 Å compared with Steidel et al. 2001 and Shapley et al. 2006, we used the spectral energy distributions (SEDs) of Bruzual & Charlot (2003) and estimated the break amplitude for $f_\nu(1500\ {\rm Å})/f_\nu(830\ {\rm Å})$ to be 3.4 based on $f_\nu(1500\ {\rm Å})/f_\nu(900\ {\rm Å}) = 3$. We assume a factor of $\sim$1.2 ($\exp(\tau_{\rm IGM,LyC})$) reduction in $f_{\rm LyC}/f_{1500}$ for the neutral hydrogen opacity in the IGM, modeled in the same manner as Madau (1995) and Siana et al. (2007). The SBC spectra measure up to rest frame $\sim$1080 Å for our targets. Therefore, to calculate the escaping UV photons at 1500 Å, we use the flux within our spectrum between rest frame 1000 and 1050 Å and apply a scaling factor (S) to estimate the flux at 1500 Å (f_{1500}). The sources in our sample are by selection blue objects with low to moderate levels of extinction. Using the SEDs of Bruzual & Charlot (2003), and assuming 0.4 solar metallicity, constant star formation with a 300 Myr old population, we derive the scaling factor to go from f_{1025} to f_{1500} to be 1.5 in f_λ. The 1000–1050 Å flux measurement does not consider the possible effect, if any, of the Lyβ λ1026 absorption line as seen in a composite spectrum of $z \sim 3$ LBGs

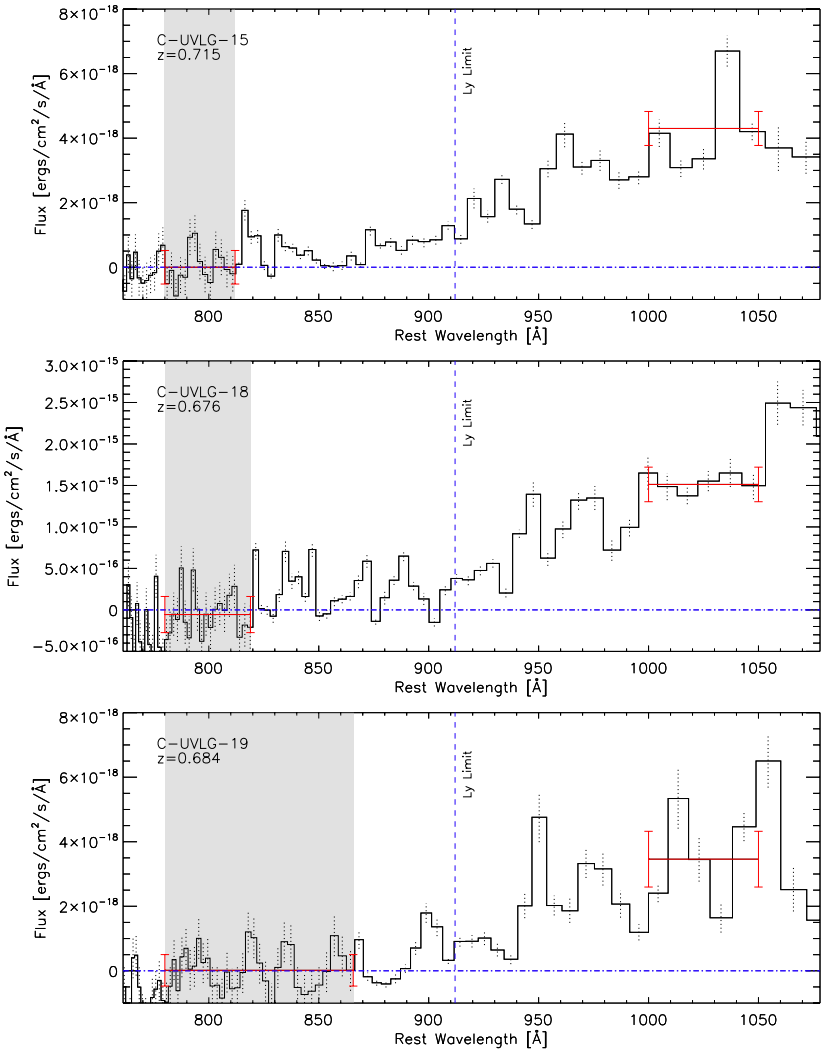

Figure 5. (Continued)

(Shapley et al. 2006). Although the spectral resolution is too low to estimate the strength of this line, it likely has little impact since our measure of the continuum flux is averaged over 50 Å. The fluxes derived from the spectra are also consistent with aperture photometry derived using the F150LP images.

As we mentioned earlier, due to the slitless nature of the spectra there is spectral smearing along the dispersion direction proportional to the spatial size of the object. A different red wavelength cutoff was assumed for each object based on the galaxy's size in the SBC direct image to ensure that light redward of the Lyman limit did not contaminate the LyC flux measurement. The sources have typical radii of ∼7–20 pixels in F150LP corresponding to a red cutoff of range of ∼820–880 Å. Furthermore, the sensitivity drops sharply at the blue end and therefore we consider only the regions at rest wavelengths > 780 Å. The final spectral region used when estimating the LyC flux is between ∼780 and 880 Å with the red cutoff changing as a function of galaxy size (shaded regions in Figure 5).

The continuum is relatively flat around 850 Å for galaxies that are actively forming stars (Bruzual & Charlot 2003), like those in our sample. We therefore integrate the observed spectrum over several resolution elements to increase the signal-to-noise ratio. The wavelength solutions of the SBC are accurate to a few angstroms between the observed 1300 Å and 1700 Å over the SBC field of view, and the flux calibrations over this wavelength range are accurate to approximately 5% (Larsen 2006). The flux below the Lyman limit (f_{830}) is taken to be the average flux between 780 and 880 Å (again the red cutoff depends on the galaxy size). The uncertainty in f_{830} is derived using the following equation:

$$f_{\mathrm{er},830} = \frac{\sqrt{\sum(\Delta f_{\mathrm{er}}^2 \times \Delta\lambda^2)}}{\Delta\lambda_{\mathrm{tot}}}, \quad (2)$$

where Δf_{er} is the standard deviation of the flux in each pixel, $\Delta\lambda$ is the size of each pixel in angstroms (this value changes as a function of wavelength), and $\Delta\lambda_{\mathrm{tot}}$ is the total wavelength range being averaged. The amount of escaping radiation below the Lyman limit is typically reported using a *relative* escape fraction (defined earlier in this section) or through a UV-to-LyC flux density ratio ($f_\nu(1500\ \text{Å})/f_\nu(830\ \text{Å})$. The former measure, however, requires an assumption for the intrinsic Lyman break which is not well constrained. In the next section, we present both the UV-to-LyC flux density ratios and the inferred relative escape fractions for completeness.

5. RESULTS

We find one detection of escaping LyC radiation in an AGN–starburst composite, but no direct detections of far-UV flux in our remaining sample of 31 $z \sim 0.7$ LBG analogs.

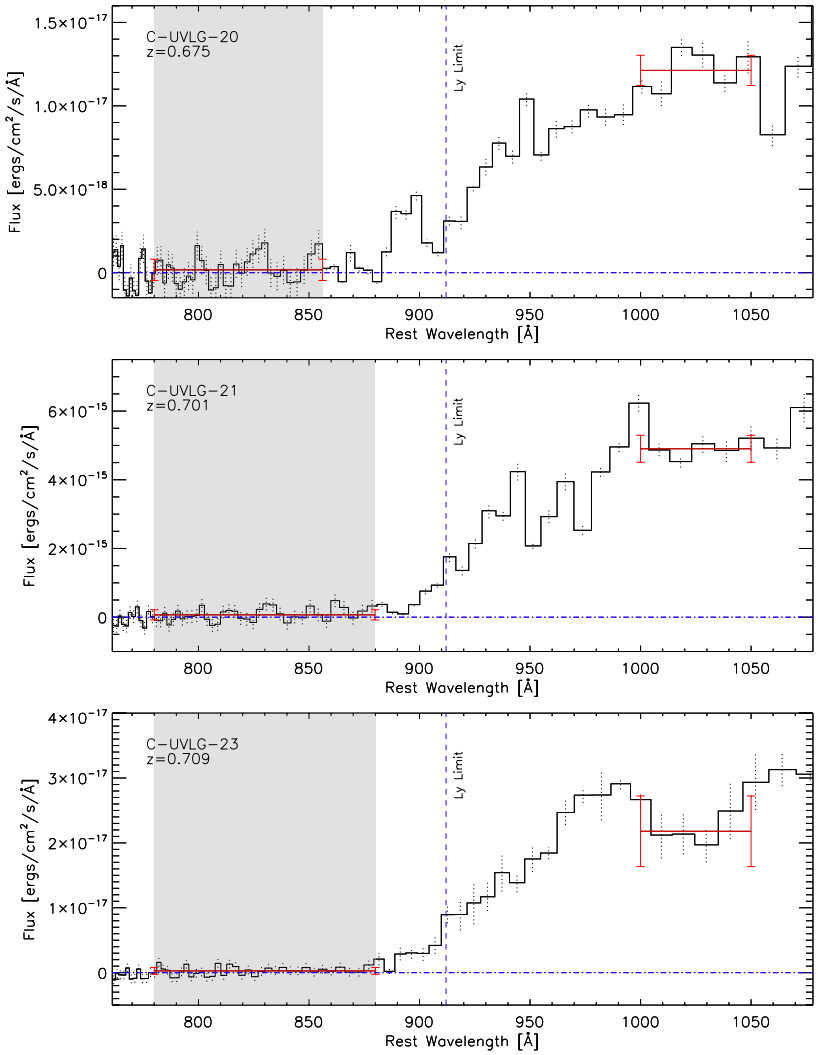

Figure 5. (Continued)

Nine galaxies (C-UVLG-3, 9, 10, 13, 14, 16, 22, 31, 32) were not detected in the direct F150LP image or PR130L spectra. Measuring limits on the LyC escape for these objects requires careful cross-calibration between *HST* and *GALEX* data due to the significant difference in angular resolutions (*GALEX* point-spread function (PSF) $\sim 5''$ in the FUV band) and will be presented in a future paper (H. I. Teplitz et al. 2010, in preparation). The non-detections are likely due in part to their large size which resulted in UV surface brightnesses below the sensitivity of our observations. Another likely contributing factor is that 7/9 of the undetected galaxies had the largest extinctions within our sample, $E(B-V) > 0.3$, based on SED fitting.

The observed flux density ratio, $f_\nu 1500/f_\nu 830$, in the individual sources range from 20 to 204 with a median of 73.5 (3σ lower limits). In order to convert these ratios into a *relative* escape fraction, we apply Equation (1) assuming an average IGM transmission of 0.85 and a value of 3.4 or 7 for the intrinsic Lyman break (see Table 1). Our far-UV sensitivities give $f_{\rm esc,rel}$ close to zero, with individual 3σ upper limits ranging from 0.01–0.19. Since we have assumed an average IGM transmission, these upper limits are likely to be even lower in the majority of these objects since the IGM opacity at low redshift is dominated by very few opaque lines of sight (Siana et al. 2007).

In order to increase our sensitivity further, we stacked the non-detections with UV sizes $\lesssim 0.''78$ in diameter, which corresponds to a red cutoff of $\sim$860 Å. This red cutoff was chosen to maximize the number of galaxies in the stack while probing as closely to the Lyman limit as possible. The stack was composed of 18 galaxies placing a 3σ lower limit on $f_\nu 1500/f_\nu 830 = 378.7$ and a 3σ upper limit of $f_{\rm esc,rel} < 0.01$ (Figure 6). In addition to the global stack, we separated the sample by morphology, stacking the eight galaxies which were visually classified in the *HST* F814W image to be undergoing a merger event and a radius of $\leqslant 0.''7$ (red cutoff of 865 Å). We find 3σ lower limits for $f_\nu 1500/f_\nu 830 = 223.2$ and a $f_{\rm esc,rel} < 0.02$ (3σ upper limit) for galaxy mergers (see Figure 7 and Section 6.3 for further discussion).

5.1. LyC Emission: AGN and Star Formation?

Flux below the Lyman limit was detected in C-UVLG-17 (hereafter T17), however, it is unclear what process is responsible for the FUV emission (Figure 4). T17 is detected in the X-ray with a luminosity of $\sim 2 \times 10^{43}$ erg s^{-1} (2–10 KeV) (Brusa et al. 2010), and is a Type 2 AGN based on the optical spectrum (Prescott et al. 2006). Although it is highly probable that the LyC flux is coming from the AGN, it is possible that some flux has its origin in young massive stars. The COSMOS photometry, with 30 bands, was fit using a library of "hybrid" templates tuned for

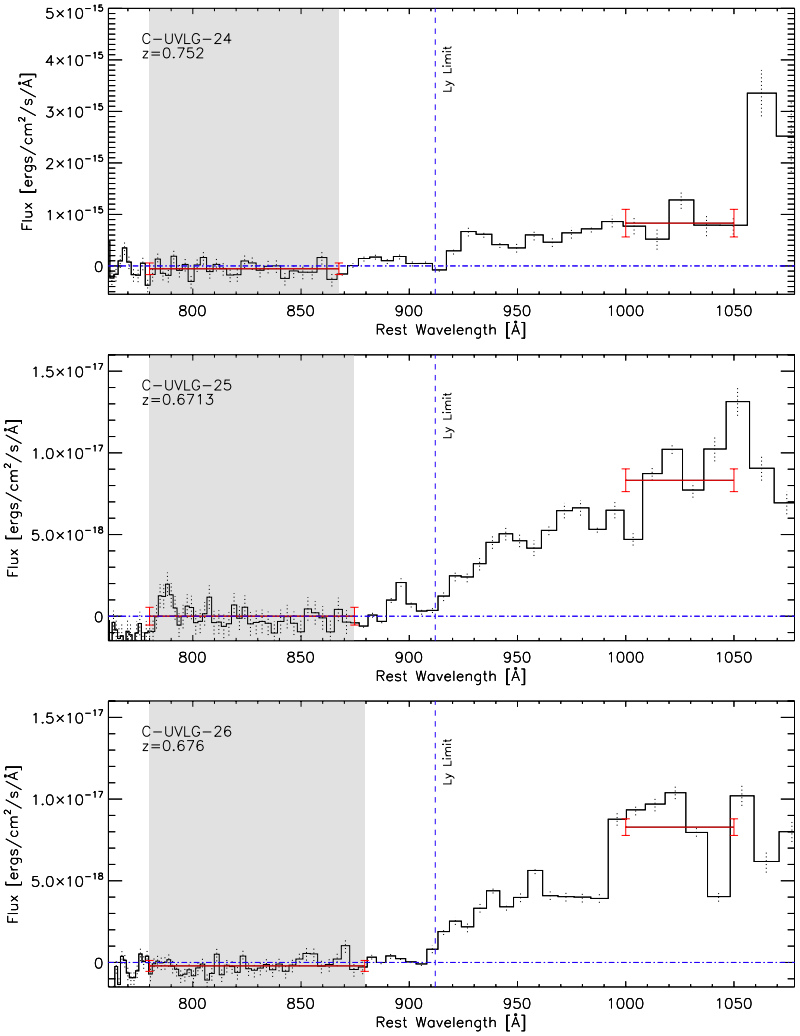

Figure 5. (Continued)

sources hosting an AGN, even if it is hidden (see Salvato et al. 2009 for details). The best-fit SED is a pure starburst, although the fit is poor. The IRAC colors do not place T17 in the locus of optically bright unobscured AGN and is non-variable (over a five year period). The spectrum shows no break at the Lyman limit, with ionizing flux detected down to $\lambda \sim 810$ Å. Below this wavelength, the continuum is strongly suppressed, indicative of a foreground, high-column density absorber at $z \sim 0.55$.

Although this source harbors an AGN, it is worth noting that a large fraction of the LyC radiation could be from the starburst, with the AGN clearing lines of sight. It is impossible to disentangle the fractional contribution of the LyC radiation from the two sources. In the context of this paper, we do not consider the LyC emission from this galaxy to be analogous to the LyC detections at high-z, although this type of LyC emission is interesting and possibly more common at higher redshift.

5.2. Foreground Contamination

Higher redshift ($z \sim 3$) studies have detected LyC photons in approximately 10% of galaxies (Shapley et al. 2006; Iwata et al. 2009). Vanzella et al. (2010) estimate that at $z \sim 3$ there is a 50% probability that 1/3 of the galaxies with detected LyC emission are the result of foreground contamination by low-redshift blue galaxies within $\sim 1''$ of the high-redshift galaxy. Figure 8 highlights an example of foreground contamination found in C-UVLG-14 of our sample. The NUV *GALEX* magnitude which is used in our sample selection has a PSF of $\sim 4''$ which encompasses both galaxies.

The high-resolution *HST* F814W image (Scoville et al. 2007) reveals two galaxies separated by $\sim 1\farcs2$ (<10 kpc), exhibiting irregular morphologies consistent with a close galaxy pair. The southern galaxy (hereafter GalA) has two compact nuclei and evidence of long tidal tails. The northern galaxy (hereafter GalB) exhibits multiple star formation knots, an asymmetric morphology, and tidal tails. The two primary UV bright knots that make up GalB are referred to as GalB1 and GalB2 as noted in Figure 8.

Although GalA was the intended target in our program ($z_{\rm spec} = 0.772$), the high-resolution SBC direct F150LP image revealed that GalB dominated the NUV and FUV flux. The *Spitzer* 24 μm detection is centered on GalA corresponding to an IR luminosity of $L_{[8-1000\,\mu{\rm m}]} = 2.3 \times 10^{11}\ L_{\odot}$ and an SFR of $\sim 40\ M_{\odot}\ {\rm yr}^{-1}$ (Kennicutt 1998). GalA was not detected in the FUV (likely due to its high dust content), however, the UV spectrum of GalB2 (Figure 9) would imply a *relative* escape fraction, $f_{\rm rel,esc}$ of 30% ± 6% and an f_{ν} (1500 Å)/f_{ν}(830 Å) = 14.3, if it was at the same redshift as GalA. Follow-up spectroscopy with Keck DEIMOS revealed that GalB (B1 and B2) was a low-redshift interloper at $z = 0.19$. The close ($\sim 1''$) projected separation of GalA and GalB is a good example of

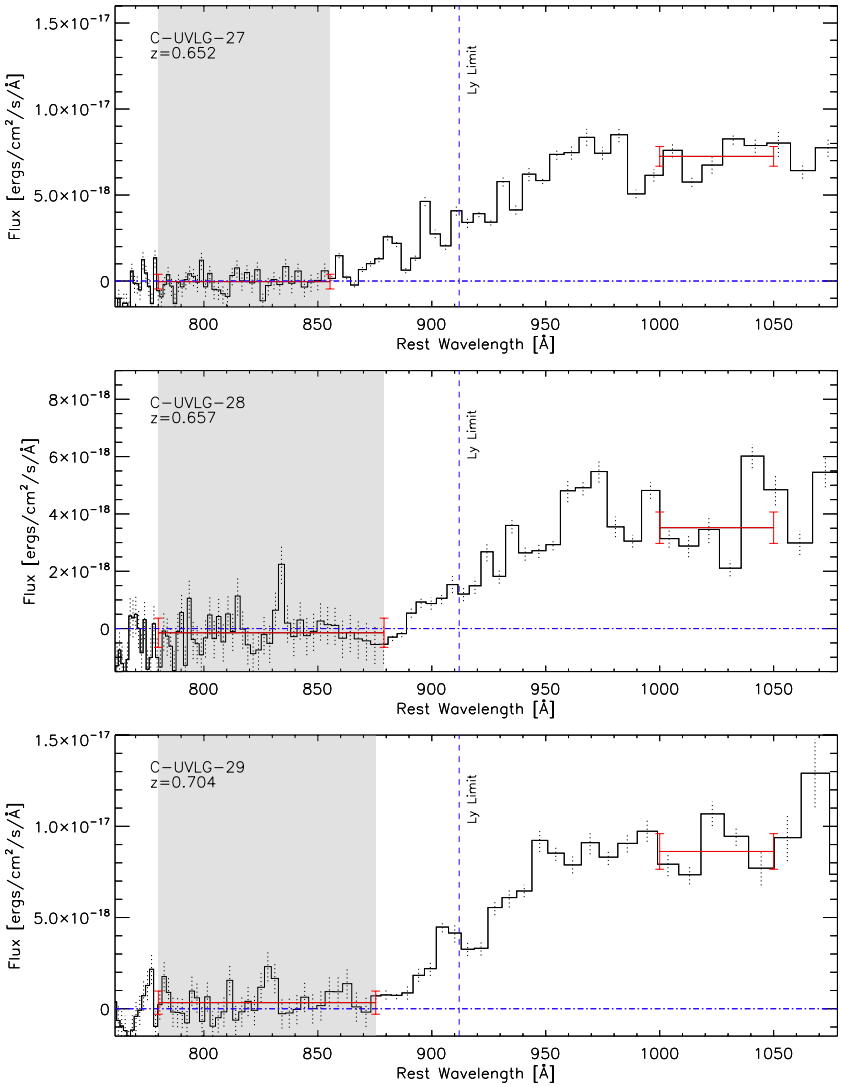

Figure 5. (Continued)

foreground contamination and could explain some of the $z \sim 3$ detections of Iwata et al. (2009), particularly the ones with a $\sim 1''$ offset between the LyC emission and assumed LBG counterpart.

6. DISCUSSION

The deep UV spectra presented here achieve the lowest individual limits of the ionizing escape fraction at any redshift. We confirm the results of shallower studies that suggest low escape fractions in moderate redshift starbursts. We now present our findings in the context of recent studies and discuss some possible mechanisms that could be responsible for the apparent lack of $z \sim 1$ starbursts with large escape fractions.

6.1. Comparison with Recent Work

Recently, Siana et al. (2010) used *HST* ACS/SBC 1500 Å imaging of 15 $z \sim 1.3$ starburst galaxies in the GOODS field, obtaining a stacked 3σ limit of $f_\nu(700)/f_\nu(1500) < 0.02$. With the inclusion of previous studies (Malkan et al. 2003; Siana et al. 2007), they state that no more than 8% of star-forming galaxies at $z \sim 1$ have relative escape fractions greater than 0.50. Cowie et al. (2009) stacked the *GALEX* far-UV (1500 Å) fluxes of a much larger sample (626 galaxies) and obtained a similar 3σ upper limit of $f_\nu(700)/f_\nu(1500) < 0.012$, confirming that starbursts at $z \sim 1$ have low ionizing emissivities. All of these studies have used broadband UV imaging to probe the LyC at $\sim$700 Å whereas the detections at $z \sim 3$ have been obtained through spectroscopy (Steidel et al. 2001; Shapley et al. 2006) and narrowband imaging (Iwata et al. 2009) where the LyC is sampled just below the Lyman limit (880–910 Å).

This is the first $z \sim 1$ spectroscopic study to provide LyC measurements much closer to the Lyman limit and is therefore more directly comparable to these higher redshift studies. Shapley et al. (2006), with a sample of 14 LBGs, probe a slightly higher UV luminosity (see Figure 10) and detect two objects with large escape fractions (with LyC-to-UV ratios significantly above our limits). One of these objects likely has a lower escape fraction than initially reported as it was not detected in deep narrowband imaging probing the LyC (Iwata et al. 2009). Therefore, only 1 of 14 objects has a significant detection. In a stack of the 12 undetected sources, Shapley et al. (2006) find an observed lower limit on the UV-to-LyC flux density ratio at $z \sim 3$ of $f_{1500}/f_{900} > 43.0$, compared to our $z \sim 1$ lower limit of $f_{1500}/f_{830} > 379$. Similarly, Iwata et al. (2009), which probe comparable rest-frame UV luminosities as our $z < 1$ sample,

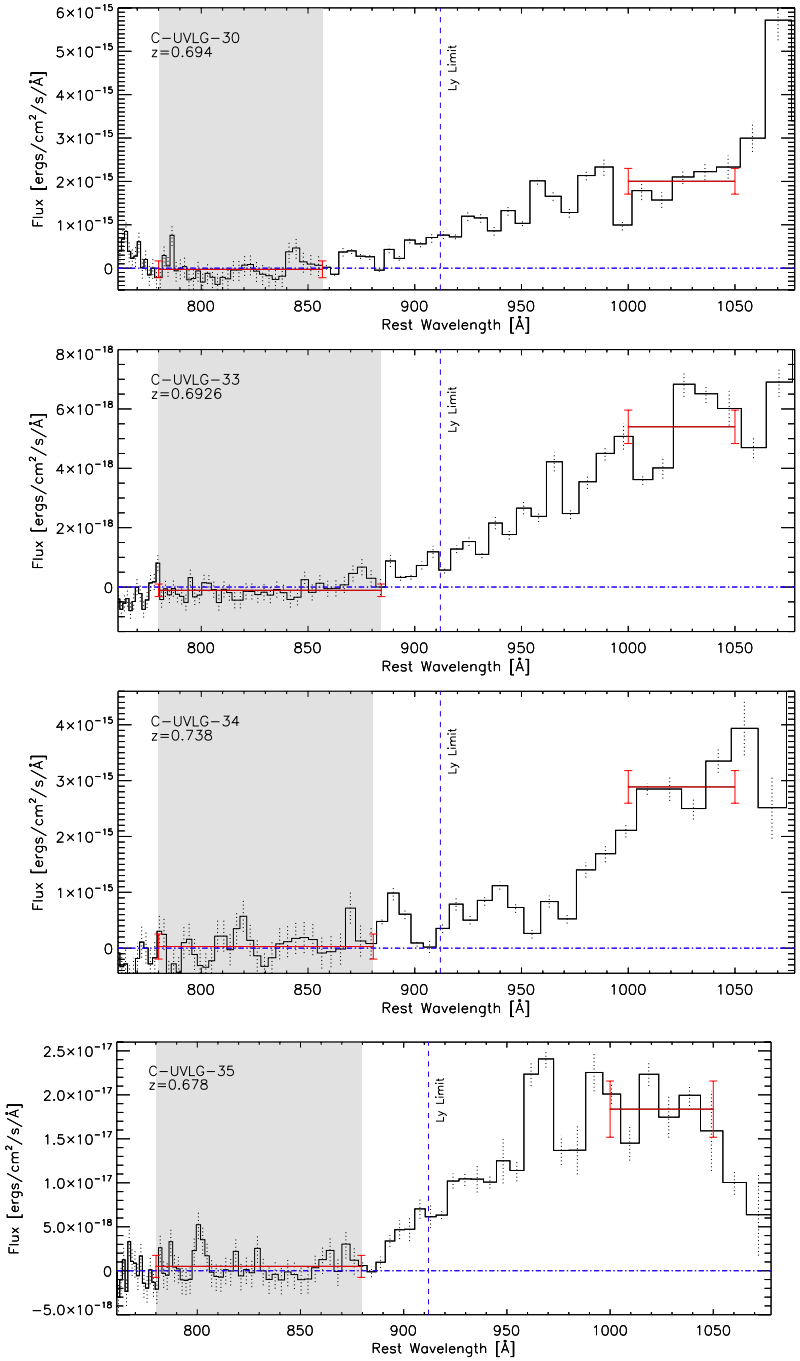

Figure 5. (Continued)

detect large escape fractions in ∼10% of LBGs and Lyα emitters at $z = 3.1$. If the LBG analogs in our sample have ionizing properties similar to LBGs at $z \sim 3$, we would expect to detect approximately three objects with large fractions of escaping LyC radiation; however, we detect none (excluding the AGN–starburst composite).

Our individual limits are significantly better than the studies at $z = 3$, so if there are significant numbers of galaxies with lower escape fractions (e.g., $f_{\rm esc,rel} \sim 0.20$, rather than unity), we would be able to detect them. We see no evidence for this scenario in our sample. Comparing our findings, which are in agreement with all other $z < 1 f_{\rm esc}$ measurements, with $z \sim 3$ studies (Shapley et al. 2006; Iwata et al. 2009) implies that the average escape fraction evolves with redshift, but the cause of this evolution remains unknown. It should be noted, however, that foreground contamination, which is likely more severe at higher redshift, may account for some of the apparent evolution seen between $z = 1$ and 3 by this work and others (Siana et al. 2010; Vanzella et al. 2010; Inoue et al. 2006). We proceed by focusing on possible mechanisms that could explain the lack of large escape fraction galaxies at $z \sim 1$.

6.2. Selecting Analogs of High $f_{\rm esc}$ LBGs

When comparing high- and low-redshift galaxy samples, there is always some degree of uncertainty regarding the true analog nature of the two populations. As discussed in Section 2 and shown in Figure 1, we selected a sample of LBG analogs

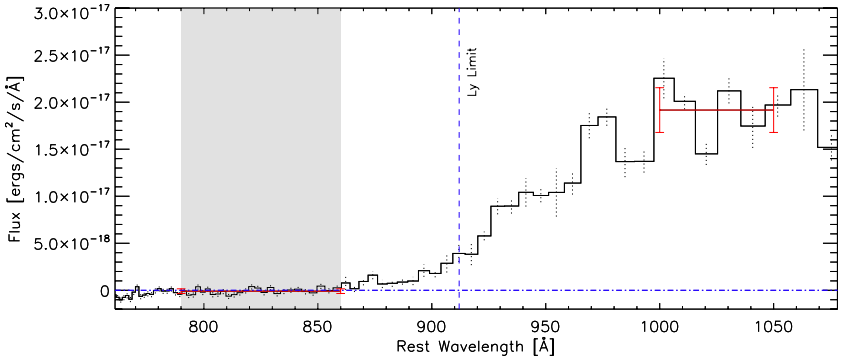

Figure 6. Stacked spectrum of 18 $z \sim 0.7$ LBG analogs. The 3σ lower limits on the observed UV-to-LyC flux density ratio is 378.7. Assuming an intrinsic Lyman break of 3.4 the upper limit on the *relative* escape fraction is 0.01 (3σ). The Lyman limit is indicated by the vertical dashed line. The horizontal lines (red) represent the average LyC and f_{1025} flux used to derive the escape fraction. Error bars are discussed in Section 3.1 and are the same as in Figure 5.

(A color version of this figure is available in the online journal.)

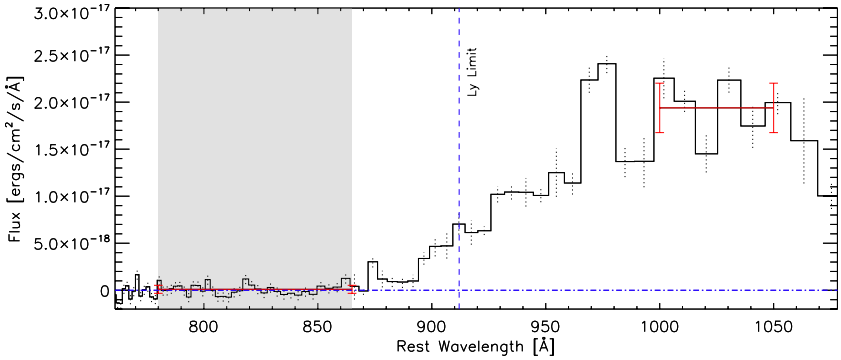

Figure 7. Stacked spectrum of 8 $z \sim 0.7$ LBG analogs with a merger morphology. The 3σ lower limits on the observed UV-to-LyC flux density ratio is 223.2. Assuming an intrinsic Lyman break of three the relative escape fraction is 0.02 (3σ). The Lyman limit is indicated by the vertical dashed line. The horizontal lines (red) represent the average flux over two wavelength ranges, 800–860 Å and 1000–1050 Å with 3σ error bars.

(A color version of this figure is available in the online journal.)

sharing many of the same properties of the Shapley et al. (2006) and Iwata et al. (2009) $z \sim 3$ LBGs. Figure 10 further highlights their similarities, showing that the distribution of reddening, stellar mass, and rest-frame UV luminosity in these sources is similar to the distribution in LBGs. The similarity in mass together with the UV–optical colors of the UVLGs implies that they may still be undergoing an early, major episode of star formation rather than a small burst on top of a hidden older population (also see Barmby et al. 2004, for the same reason applied to LBGs).

Ultimately, this sample of LBG analogs shares numerous similarities to the parent LBG population, but since only ∼10%–15% of LBGs have been observed with significant LyC detections, perhaps this subclass of LBGs has other processes at work allowing or aiding in the escape of LyC photons.

6.3. Galaxy Mergers

Galaxy mergers offer an intriguing explanation for the increased escape fraction seen at $z \sim 3$. Overzier et al. (2008) noted that UVLGs typically exhibit faint tidal features suggestive of a merger or recent interaction. They therefore propose that the super starbursts in LBGs are triggered by gas-rich mergers. Similarly, Petty et al. (2009) showed that 20%–30% of LBGs have structures akin to local starburst mergers and may be driven by similar processes.

As galaxies collide, strong gravitational and tidal forces can expel long streams of stars, and ignite violent starbursts at rates of a few to hundreds of $M_{\odot}$ yr^{-1} (Schweizer 1982; Barton et al. 2000; Bridge et al. 2010). During a merger, the tidal fields distort the galaxies radially, drawing out galactic material into long tails, plumes, and bridges (e.g., Toomre & Toomre 1972; Mihos & Hernquist 1996). The H I reservoirs can become disturbed, and the neutral gas pulled away from the sources of ionizing radiation producing low-column density lines of sight (Hibbard et al. 2000; de Mello et al. 2008) through the galaxies, in turn allowing the escape of LyC photons. Simulations by Gnedin et al. (2008) suggest that the escape fraction in major mergers can be large ($f_{\rm esc,rel} \gtrsim 30\%$) compared to non-mergers ($f_{\rm esc,rel} < 10\%$) along specific lines of sight. Within our sample of 32 galaxies, 11 had morphologies consistent with merger activity. We independently stacked eight of these spectra (removing three due to their larger spatial extent) and find $f_{\rm esc,rel} < 2\%$ (3σ upper limit).

If merging is a viable mechanism for clearing pathways in the ISM for LyC photons, the orientation of the system along the line of sight is also a likely factor, requiring a large sample of UV luminous mergers. Therefore, we cannot say whether mergers are an important factor as our sample size is at present too small. Currently, there is a lack of deep high-resolution rest-frame optical imaging of the LBGs with larger escape fractions, and the interpretation of UV morphologies remains problematic (Law et al. 2007). Future near-IR observations with *HST* of the $z \sim 3$ LBG leakers will shed light on this hypothesis.

As discussed earlier in the section, galaxy mergers are capable of clearing pathways, exposing UV bright stars. If mergers do facilitate the escape of LyC radiation then an evolving merger rate may be responsible for the observed evolution in $f_{\rm esc,rel}$. Numerous observational studies and simulations have

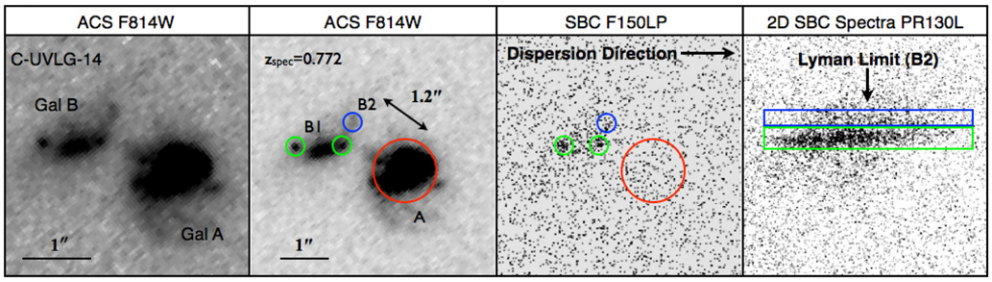

Figure 8. Postage stamp images, left to right, are *HST* F814W zoomed in followed by F814W, SBC FUV F150LP, and the FUV 2D spectra. Galaxy A (GalA) and Galaxy B (GalB) are noted in the images. The FUV flux and sites of escaping LyC are concentrated in knots (highlighted by circles) in GalB and are referred to in the text as GalB1 and GalB2. Boxes approximate the extraction regions of the UV spectra in the 2D spectral image. Flux below the Lyman limit (assuming a $z = 0.772$) is seen to the right of the arrow in both GalB1 and GalB2. However, optical spectroscopic follow-up of GalB (including both UV knots GalB1 and GalB2) revealed that it is in fact a low redshift galaxy at $z = 0.19$.

(A color version of this figure is available in the online journal.)

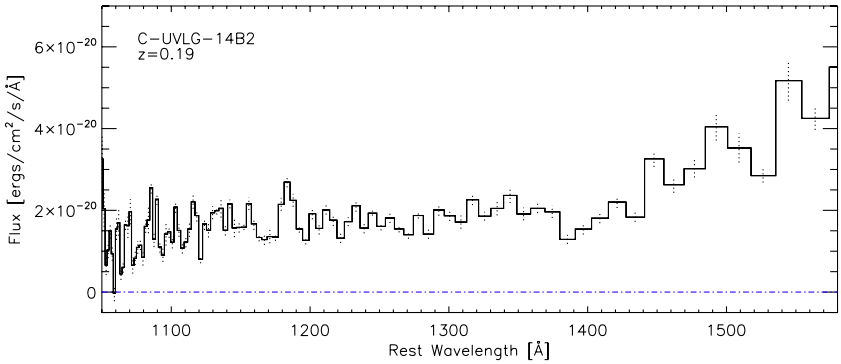

Figure 9. One-dimensional rest-frame UV spectra of GalB2, a low-redshift interloper at $z = 0.19$.

(A color version of this figure is available in the online journal.)

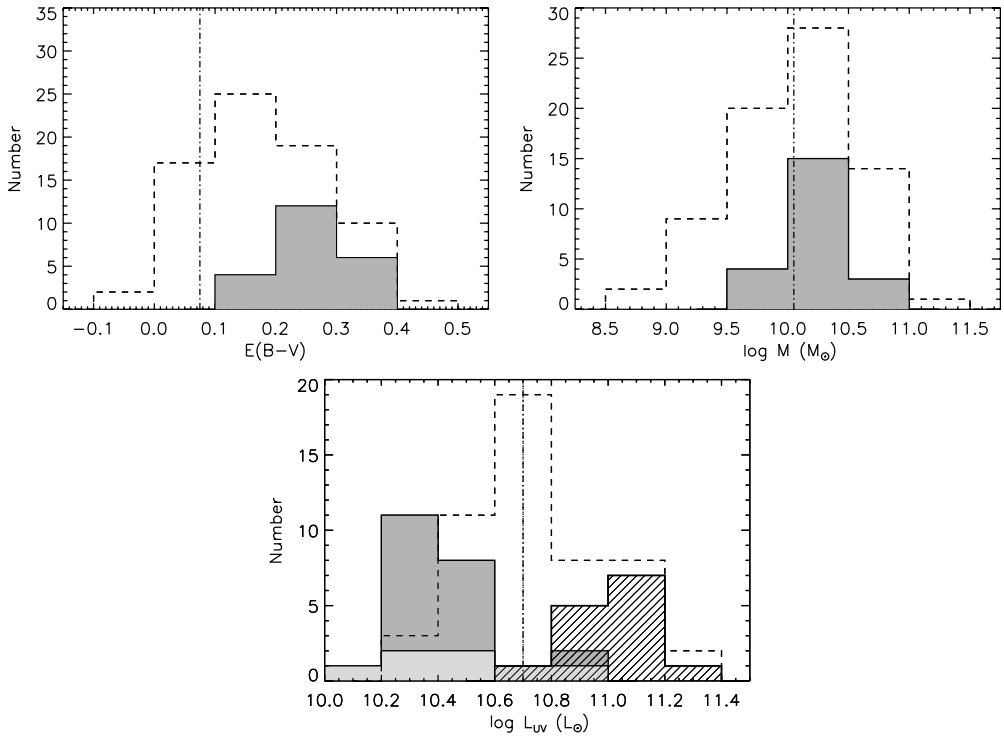

Figure 10. Histograms of extinction (left), stellar mass (right), and rest-frame UV luminosity (bottom) for the 22 local LBG analogs with measurable escape fractions. The darker shaded regions highlight the 22 galaxies presented in Table 1. A sample of $z \sim 3$ LBGs (dashed lines) in all three panels are taken from Shapley et al. (2005). The dash-dotted vertical lines show the average extinction (Verma et al. 2007) and stellar mass (Yan et al. 2006) for $z \gtrsim 5$ galaxies and the typical L_* for $z \sim 6$ galaxies (Bouwens et al. 2006). (Bottom) The seven direct detections of LyC flux in LBGs reported in Iwata et al. (2008) are denoted by the lighter shaded histogram, and the lined (angled) histogram shows the $z \sim 3$ LBG sample of Shapley et al. (2006). The extinction and stellar mass for the COSMOS sources were estimated in the photometric redshift fitting (Mobasher et al. 2007), and the UV luminosity from the *GALEX* NUV (Zamojski et al. 2007). The histograms show that the galaxies presented in this paper have low levels of extinction, similar stellar masses, and rest-frame UV luminosities compared to $z \sim 3$ LBGs.

shown that the galaxy merger rate evolves with redshift, going as $\sim(1+z)^{2-3}$ (Gottlöber et al. 2001; Conselice et al. 2008, 2003; Kartaltepe et al. 2007; Hopkins et al. 2007; Bridge et al. 2007, 2010). The factor of 3–4 increase in merger rate between $z \sim 1$ and 3 as seen observationally would also increase the number of lines of sights and range of encounter parameters observed in $z \sim 3$ galaxy mergers by the same factor. This would in turn increase the likelihood of detecting LyC at higher redshift.

6.4. Evolving $f_{\rm esc,rel}$: Size, Mass, and Star Formation

The LyC escape fraction is limited by the distribution of neutral hydrogen along a line of sight and likely depends on galactic parameters. We now consider what galaxy properties could evolve with redshift that reduce the efficiency of galactic outflows/chimneys in leaking LyC photons from luminous galaxies.

Typical galaxies (including UV bright galaxies) have been shown to be 1.5–3 times smaller at $z \sim 3$ than their local counterparts (Trujillo et al. 2006; Papovich & Bell 2002; Ferguson et al. 2004). Although our sample was selected to have similar UV surface brightnesses as $z \sim 3$ LBGs (refer to Figure 1), little is known about the true optical sizes of LBGs or the gas distribution. The velocities of galactic winds or outflows have been found to be proportional to the SFR in LBGs (Ferrara & Ricotti 2006), therefore LBG and LBG analogs, having similar SFR should in principle generate outflows with similar velocities (a few hundred km s^{-1}). However, smaller galaxies would have higher SFRs per unit volume, which can result in more efficient galactic winds (Veilleux et al. 2005), more easily clearing pathways or "chimney-like" structures, and in turn allowing for higher $f_{\rm esc,rel}$ (Fujita et al. 2003).

With smaller galaxies and higher-density starbursts come the potential for a larger fraction of stars born in very compact star clusters, including super star clusters (SSCs). SSCs can have thousands of young (<50 Myr) stars within a half-light radius of ~10 pc (Veilleux et al. 2005). These extreme concentrations of hot O and B stars can greatly impact the state of the ISM driving powerful galactic winds (like those seen in M82), opening channels for LyC photons to escape. SSCs have been detected in the tidal tails (Charlton et al. 2009) and outer regions of galaxies, which could explain the spatially offset LyC emission (to the optical emission) detected by Iwata et al. (2009) in a few $z \sim 3$ LBGs. There is also some evidence that SSCs found in the local group of galaxies have top-heavy initial mass functions (IMFs; Harayama et al. 2008), which enhance the efficiency in clearing lines of sight, due to the larger outflow velocities generated by massive stars.

Another property that has been shown to possibly evolve with redshift is the stellar mass-to-dark matter ratio. Recent work by Epinat et al. (2010) and P. Capak (2009, private communication) has reported that local massive galaxies have more centrally concentrated dark matter than higher redshift galaxies ($z \sim 0.7$) with comparable stellar masses. A higher stellar mass-to-dark-matter mass ratio at lower redshift would result in a larger gravitational potential, and in turn the requirement for larger galactic winds to achieve the same "porosity" of the ISM (reducing the probability for ionizing photons to escape their host galaxies). Thicker disks due to dense concentrations of gas have also been shown to impede or slow the development of galactic outflows, due to a higher gravitational potential (Cooper et al. 2008).

6.5. Intrinsic LyC-to-UV Ratio: A Top-heavy IMF?

An evolving intrinsic LyC-to-UV flux density ratio could also be responsible for the observed evolution in $f_{\rm esc,rel}$. The escape fraction is measured by comparing the UV (1500 Å) flux of a galaxy to flux below the Lyman limit. One key assumption that is made involves the inherent LyC-to-UV ratio of starbursts. Typically, this ratio is considered constant with redshift, but if there were an order of magnitude larger production rate of the LyC relative to the 1500 Å flux at $z > 3$ than at $z < 1$, the observed change in $f_{\rm esc,rel}$ would be expected.

Iwata et al. (2009) found that three of the six LBGs with detected escaping LyC in their sample had SEDs intrinsically bluer than those expected from population synthesis models, assuming a standard IMF with moderate dust attenuation. They show that an intrinsically bluer SED (~0.3 mag bluer in NB359-R than those of Starburst99), in the absence of QSO activity, can be produced with a top-heavy IMF. They also suggest that a deviation from the Calzetti et al. (2000) dust attenuation law, with less dust absorption at 900 Å, compared to that at 1500 Å, can come close to achieving the observed bluer colors of those LBGs.

It has been shown that the UV luminosity density at $z \sim 6$ may be insufficient to explain the ionized universe at $z > 7$ unless the IMF allowed for the production of more massive stars (Chary 2008). A top-heavy IMF at higher redshift could help explain the larger number of LyC detections at $z \sim 3$ as massive stars produce more LyC photons, and stronger supernova driven winds. A top-heavy IMF requires regions of potentially low-metallicity gas which is consistent with the metallicity and dust evolution seen from $z \sim 3$ to 1 (Ferguson et al. 2002).

7. SUMMARY

LyC photons produced in massive starbursts likely played an important role in the reionization of the universe. However, their contribution depends upon the fraction of ionizing radiation that can escape the high-column density of H I gas surrounding these star-forming galaxies. We have presented *HST* rest-frame UV slitless spectroscopy of 32 $z \sim 0.7$ LBG analogs in the COSMOS field to investigate the LyC escape fraction. These UV spectra have achieved the deepest limits to date on the escape fraction in individual sources at any redshift. A summary of our results is as follows.

Aside from the detection of leaking LyC from an AGN–starburst composite, we find no detections of LyC in our sample of 31 star-forming galaxies. The individual 3σ lower limits of the $f_\nu(1500\ \text{Å})/f_\nu(830\ \text{Å})$ ratio range from 20 to 204 (median of 73.5) and 378.7 in the stack of 18 galaxies. Assuming an intrinsic Lyman break of 3.4 and an IGM transmission of 85%, we report a *relative* escape fraction in individual galaxies of 0.02–0.19 and 0.01 in the stack (3σ upper limit). There is no indication of the near unity escape fractions found at $z \sim 3$. The striking contrast between the nearly zero escape fractions found in the 22 $z \sim 0.7$ LBG analogs with the near unity escape fractions discovered in 10% of the $z \sim 3$ LBG population strongly argues for an evolving escape fraction. It is unclear, however, if the lack of near unity escape fraction detections at low redshift is due to an evolution in the actual value of the $f_{\rm esc,rel}$ itself, or if it is just that the number of galaxies that in fact have large amounts of leaking LyC decrease with redshift. Both scenarios could explain the absence of galaxies with larger amounts of leaking LyC. Possible causes for a change in the perceived escape fraction with redshift involve a top-heavy IMF,

larger SFR densities, stellar mass-to-dark matter ratios, and/or fraction of SSCs at higher redshifts. All these mechanisms enhance the efficiency of galaxy winds, increasing the porosity of the ISM, facilitating LyC escape. However, if galaxy mergers aid in the escape of LyC radiation, then an evolving galaxy merger rate could account for the high number of LyC leaking galaxies at $z \sim 3$. The lack of low-redshift galaxies with escaping LyC could then be explained by the small number of galaxy mergers that have been observed below the Lyman limit. An additional consideration is that a fraction of the detections of escaping LyC at $z \sim 3$ may be a consequence of foreground contamination, which would reduce the strength of the evolution in $f_{\rm esc,rel}$ seen when comparing to low-z studies.

The escape fraction of UV radiation in $z \sim 1$ luminous starburst galaxies is an important quantity to understand since it provides insight into the sources (massive star formation or QSOs) responsible for reionization. Our study has presented a robust measure of the $f_{\rm esc,rel}$ in the low-redshift universe and suggests that the escape fraction in objects that are analogous to $z \sim 3$ LBG population evolves with redshift. However, future study is required to isolate the cause of this evolution.

We thank Mark Dickinson and Colin Borys for their contributions to this work and the anonymous referee for their constructive comments which added to the clarity of this paper. The research described in this paper was carried out, in part, by the Jet Propulsion Laboratory, California Institute of Technology, and observations obtained at the Hale Telescope, Palomar Observatory as part of a continuing collaboration between the California Institute of Technology, NASA /JPL, and Cornell University. Support for programs HST-GO 11236 was provided by NASA through grants from the Space Telescope Science Institute, which is operated by the Association of Universities for Research in Astronomy, Inc.

REFERENCES

Barmby, P., et al. 2004, ApJS, 154, 97
Barton, E. J., Geller, M. J., & Kenyon, S. J. 2000, ApJ, 530, 660
Bertin, E., & Arnouts, S. 1996, A&AS, 117, 393
Bouwens, R. J., Illingworth, G. D., Blakeslee, J. P., & Franx, M. 2006, ApJ, 653, 53
Bridge, C. R., Carlberg, R. G., & Sullivan, M. 2010, ApJ, 709, 1067
Bridge, C. R., et al. 2007, ApJ, 659, 931
Brusa, M., et al. 2009, ApJ, 693, 8
Brusa, M., et al. 2010, ApJ, 718, 348
Bruzual, G., & Charlot, S. 2003, MNRAS, 344, 1000
Calzetti, D., Armus, L., Bohlin, R. C., Kinney, A. L., Koornneef, J., & Storchi-Bergmann, T. 2000, ApJ, 533, 682
Charlton, J. C., et al. 2009, BAAS, 41, 479
Chary, R.-R. 2008, ApJ, 680, 32
Conselice, C. J., Bershady, M. A., Dickinson, M., & Papovich, C. 2003, AJ, 126, 1183
Conselice, C. J., Rajgor, S., & Myers, R. 2008, MNRAS, 386, 909
Cooper, J. L., Bicknell, G. V., Sutherland, R. S., & Bland-Hawthorn, J. 2008, ApJ, 674, 157
Cowie, L. L., Barger, A. J., & Trouille, L. 2009, ApJ, 692, 1476
de Mello, D. F., Smith, L. J., Sabbi, E., Gallagher, J. S., Mountain, M., & Harbeck, D. R. 2008, AJ, 135, 548
Deharveng, J.-M., Buat, V., Le Brun, V., Milliard, B., Kunth, D., Shull, J. M., & Gry, C. 2001, A&A, 375, 805
Epinat, B., Amram, P., Balkowski, C., & Marcelin, M. 2010, MNRAS, 401, 2113
Ferguson, H. C., Dickinson, M., & Papovich, C. 2002, ApJ, 569, L65
Ferguson, H. C., et al. 2004, ApJ, 600, L107
Ferrara, A., & Ricotti, M. 2006, MNRAS, 373, 571
Fujita, A., Martin, C. L., Mac Low, M.-M., & Abel, T. 2003, ApJ, 599, 50
Giallongo, E., Fontana, A., & Madau, P. 1997, MNRAS, 289, 629
Giavalisco, M. 2002, ARA&A, 40, 579
Glikman, E., Bogosavljević, M., Djorgovski, S. G., Stern, D., Dey, A., Jannuzi, B. T., & Mahabal, A. 2010, ApJ, 710, 1498
Gnedin, N. Y., Kravtsov, A. V., & Chen, H.-W. 2008, ApJ, 672, 765
Gottlöber, S., Klypin, A., & Kravtsov, A. V. 2001, ApJ, 546, 223
Harayama, Y., Eisenhauer, F., & Martins, F. 2008, ApJ, 675, 1319
Heckman, T. M., et al. 2005, ApJ, 619, L35
Hibbard, J. E., Vacca, W. D., & Yun, M. S. 2000, AJ, 119, 1130
Hoopes, C. G., et al. 2007, ApJS, 173, 441
Hopkins, P. F., Bundy, K., Hernquist, L., & Ellis, R. S. 2007, ApJ, 659, 976
Inoue, A. K., Iwata, I., & Deharveng, J.-M. 2006, MNRAS, 371, L1
Iwata, I., et al. 2009, ApJ, 692, 1287
Jiang, L., et al. 2008, AJ, 135, 1057
Kartaltepe, J. S., et al. 2007, ApJS, 172, 320
Kennicutt, R. C., Jr. 1998, ARA&A, 36, 189
Koekemoer, A. M., et al. 2007, ApJS, 172, 196
Kümmel, M., Larsen, S. S., & Walsh, J. R. 2006, in The 2005 *HST* Calibration Workshop: *Hubble* After the Transition to Two-Gyro Mode, ed. A. M. Koekemoer, P. Goudfrooij, & L. L. Dressel (Washington, DC: NASA), 85
Larsen, S. S. 2006, Wavelength and Flux calibration of the ACS/SBC PR110L and PR130L Prisms, Technical Report
Larsen, S. S., Walsh, J., & Kummel, M. 2006, Wavelength and Flux Calibration of the ACS/HRC PR200L Prism, Technical Report
Law, D. R., Steidel, C. C., Erb, D. K., Pettini, M., Reddy, N. A., Shapley, A. E., Adelberger, K. L., & Simenc, D. J. 2007, ApJ, 656, 1
Leitherer, C., Ferguson, H. C., Heckman, T. M., & Lowenthal, J. D. 1995, ApJ, 454, L19
Lilly, S. J., et al. 2009, ApJS, 184, 218
Madau, P. 1995, ApJ, 441, 18
Madau, P., Haardt, F., & Rees, M. J. 1999, ApJ, 514, 648
Malkan, M., Webb, W., & Konopacky, Q. 2003, ApJ, 598, 878
Mihos, J. C., & Hernquist, L. 1996, ApJ, 464, 641
Mobasher, B., et al. 2007, ApJS, 172, 117
Oke, J. B., & Gunn, J. E. 1982, PASP, 94, 586
Overzier, R. A., et al. 2008, ApJ, 677, 37
Papovich, C., & Bell, E. F. 2002, ApJ, 579, L1
Petty, S. M., de Mello, D. F., Gallagher, J. S., Gardner, J. P., Lotz, J. M., Matt Mountain, C., & Smith, L. J. 2009, AJ, 138, 362
Prescott, M. K. M., Impey, C. D., Cool, R. J., & Scoville, N. Z. 2006, ApJ, 644, 100
Salvato, M., et al. 2009, ApJ, 690, 1250
Schweizer, F. 1982, ApJ, 252, 455
Scoville, N., et al. 2007, ApJS, 172, 38
Shapley, A. E., Steidel, C. C., Erb, D. K., Reddy, N. A., Adelberger, K. L., Pettini, M., Barmby, P., & Huang, J. 2005, ApJ, 626, 698
Shapley, A. E., Steidel, C. C., Pettini, M., Adelberger, K. L., & Erb, D. K. 2006, ApJ, 651, 688
Siana, B., et al. 2007, ApJ, 668, 62
Siana, B., et al. 2008, ApJ, 675, 49
Siana, B., et al. 2010, arXiv:1001.3412
Steidel, C. C., Pettini, M., & Adelberger, K. L. 2001, ApJ, 546, 665
Teplitz, H. I., et al. 2006, AJ, 132, 853
Toomre, A., & Toomre, J. 1972, ApJ, 178, 623
Trujillo, I., et al. 2006, ApJ, 650, 18
Vanzella, E., Siana, B., Cristiani, S., & Nonino, M. 2010, MNRAS, 404, 1672
Veilleux, S., Cecil, G., & Bland-Hawthorn, J. 2005, ARA&A, 43, 769
Verma, A., Lehnert, M. D., Förster Schreiber, N. M., Bremer, M. N., & Douglas, L. 2007, MNRAS, 377, 1024
Walsh, J. R., Kümmel, M., & Larsen, S. S. 2006, in The 2005 *HST* Calibration Workshop: *Hubble* After the Transition to Two-Gyro Mode, ed. A. M. Koekemoer, P. Goudfrooij, & L. L. Dressel (Washington, DC: NASA), 79
Willott, C. J., et al. 2010, AJ, 139, 906
Yan, H., Dickinson, M., Giavalisco, M., Stern, D., Eisenhardt, P. R. M., & Ferguson, H. C. 2006, ApJ, 651, 24
Zamojski, M. A., et al. 2007, ApJS, 172, 468